

Normal State Spin Dynamics of Five-band Model for Iron-pnictides

Toshikaze KARIYADO and Masao OGATA

*Department of Physics, Graduate School of Science, University of Tokyo, 7-3-1, Bunkyo-ku, Tokyo 113-0033
JST, TRIP, 5 Sanbancho, Chiyoda, Tokyo 102-0075*

Normal state spin dynamics of the recently discovered iron-pnictide superconductors is discussed by calculating spin structure factor $S(q, \omega)$ in an itinerant five-band model within RPA approximation. Due to the characteristic Fermi surface structure of iron-pnictide, column like response is found at $(\pi, 0)$ in extended Brillouin zone in the undoped case, which is consistent with the recent neutron scattering experiment. This indicates that the localized spin model is not necessary to explain the spin dynamics of this system. Furthermore, we show that the temperature dependence of inelastic neutron scattering intensity can be well reproduced in the itinerant model. We also study NMR $1/T_1T$ in the same footing calculation and show that the itinerant model can capture the magnetic property of iron-pnictide superconductors.

KEYWORDS: iron-pnictide, multi-orbital Hubbard model, inelastic neutron scattering, NMR

Recently discovered¹⁾ iron-pnictide (or transition-metal pnictide) superconductors have attracted much attention and have been studied intensively since they show superconductivity at rather high temperatures up to $55\text{K}^{2,3)}$ at present. Novelty of this series of compounds is not limited to their high T_c : entangled band structure, coexistence of hole and electron Fermi surfaces,^{4,5)} origin of the magnetism,^{6,7)} interplay between magnetism and superconductivity,^{8,9)} role of lattice structure,^{10,11)} nodal or nodeless behavior in the superconducting phase,¹²⁻¹⁵⁾ robustness against impurities in the conducting layer¹⁶⁻¹⁸⁾ and so on. All of these features enrich the physics of this compound. In this paper, we pay attention to magnetic properties of this series of compounds, especially the normal state spin dynamics.

For the study of spin dynamics, NMR and inelastic neutron scattering experiments are powerful tools. There already exist systematic works of NMR,^{12,19)} and some results of inelastic neutron scattering on iron-pnictides.²⁰⁻²⁴⁾ The normal state behavior of $1/T_1T$ obtained in the NMR shows a clear tendency against electron doping. In the low doping region, which is near the magnetically ordered phase, one can see enhancement of $1/T_1T$ with decreasing temperature, while in the high doping region, there is no enhancement of $1/T_1T$ and rather, it decreases with decreasing temperature. On the other hand, in the inelastic neutron scattering experiments, at least two common features have been observed: one is column-like response at the antiferromagnetic wavenumber and another is gapped spin excitation spectra.

Analysis of these results in the inelastic neutron scattering is often carried out with a Heisenberg-type spin model,^{25,26)} although this system shows itinerancy. Sometimes this system is regarded as a bad metal, but

it is basically metallic in transport properties²⁷⁾ (at most semiconducting). In addition, ARPES measurements show that the band structure coincides with those obtained in the first principle calculation with a mass renormalization factor of 2-4.^{28,29)} This means that, although electron correlation plays important role in the iron-pnictides, it is not so strong as in the high T_c cuprates, whose mother compounds are well described by a localized-spin Heisenberg model. Thus, in this paper we analyze the inelastic neutron measurements based on a purely itinerant model. We also discuss NMR results of $1/T_1T$ briefly to be more concrete.

The model we use is the five-band Hubbard model proposed by Kuroki *et al.*⁵⁾ which is down-folded from the first principle calculation. Five bands in this model mainly comes from five Fe-3d orbitals and hopping parameters are kept up to fifth nearest neighbor. The dispersion relation and the structure of the density of states are in good agreement with the first principle calculation. Although this model is two-dimensional, this simplification is not so harmful since the Fermi surfaces of this system are basically cylindrical. We must also note that this model contains one Fe atom per unit cell and Brillouin zone is doubled compared with the original one. (See upper panel of Fig. 1.) Actually, this model is constructed from LaFeAsO system, but we believe that the properties of FeAs layer is qualitatively same for other types of iron-pnictide. The interaction is limited to the onsite interaction and treated within RPA approximation. We tried several sets of interaction parameters keeping the constraints of $U = U' + J + J'$ and $J = J'$, but the results shown in the following are those with $U = 1.1$, $U' = 0.9$, $J = 0.1$ and $J' = 0.1$. Here, the unit of the energy is electron volt (eV). We treat doping as a rigid band shift, i.e., we neglect possible structural change due to the change

of the charge balance between the conduction layers and blocking layers. Note that $n = 6.0$ corresponds to the stoichiometric sample in this model. We divide Brillouin zone into 64×64 meshes and 1024 Matsubara frequencies are used. Padé approximation is used to transform the results on Matsubara frequencies to those on real frequency.

In order to analyze the inelastic neutron scattering experiments, we calculate spin structure factor $S(\mathbf{q}, \omega)$, which is defined as Fourier transform of a spin correlation function,

$$S(\mathbf{q}, \omega) = \frac{1}{N} \sum_{\mathbf{r}} e^{-i\mathbf{q} \cdot \mathbf{r}} \int_{-\infty}^{\infty} dt e^{-i\omega t} \langle \hat{S}_0 \cdot \hat{S}_{\mathbf{r}}(t) \rangle. \quad (1)$$

To be precise, we must include a form factor, often denoted as $F(\mathbf{q})$, in the above definition for the comparison with experimentally obtained scattering cross section. However, we ignore them since we believe that they do not change the following conclusion. In the spin-isotropic case, we calculate

$$\chi^{+-}(\mathbf{q}, i\omega_n) = \int_0^\beta d\tau e^{i\omega_n \tau} \langle \hat{S}_{-\mathbf{q}}^+(\tau) \hat{S}_{\mathbf{q}}^- \rangle \quad (2)$$

where $\hat{S}_{\mathbf{q}}^+$ is defined as

$$\hat{S}_{\mathbf{q}}^+ = \frac{1}{N} \sum_{\mathbf{k}} \sum_a c_{\mathbf{q}+\mathbf{k}a\uparrow}^\dagger c_{\mathbf{k}a\downarrow}, \quad (3)$$

and a denotes the orbital indices. Then, $S(\mathbf{q}, \omega)$ is obtained using the fluctuation-dissipation theorem as

$$S(\mathbf{q}, \omega) = \frac{\text{Im}\chi^{+-}(\mathbf{q}, \omega)}{1 - e^{-\beta\omega}}. \quad (4)$$

The main panel of Fig. 1 shows the overall view of $S(\mathbf{q}, \omega)$ calculated at $n = 6.0$ and temperature $T = 0.02\text{eV}$ along the high symmetry lines of the Brillouin zone shown in Fig. 1 (a). Note that the energy range is beyond the experimental reach. We can see two prominent features in this figure: one is the peak at $\mathbf{q} \sim (\pi, \pi)$ and $\omega \sim 1\text{eV}$ and another is the peak at $\mathbf{q} \sim (\pi, 0)$ and $\omega \sim 0\text{eV}$. Considering the DOS (shown in the inset of the main panel of Fig. 1) and dispersion relations, we can see that the former corresponds to a transition between two van Hove singularities above and below the Fermi energy. The latter peak comes from the nesting of the Fermi surface. Remember that the wave vector $(\pi, 0)$ in the present model corresponds to (π, π) in the original Brillouin zone (Fig. 1(b)).

The low energy part of $S(\mathbf{q}, \omega)$ is shown in Fig. 2 to compare with experimental results. We can see that the intensity distributions above $(\pi, 0)$ are almost vertical in this energy range, which is similar to the experimentally observed $S(\mathbf{q}, \omega)$. Quite often, the column-like response at $(\pi, 0)$ is interpreted by localized spin model. However, the present results indicates that the localized spin model is not necessary to explain the spin dynamics of this sys-

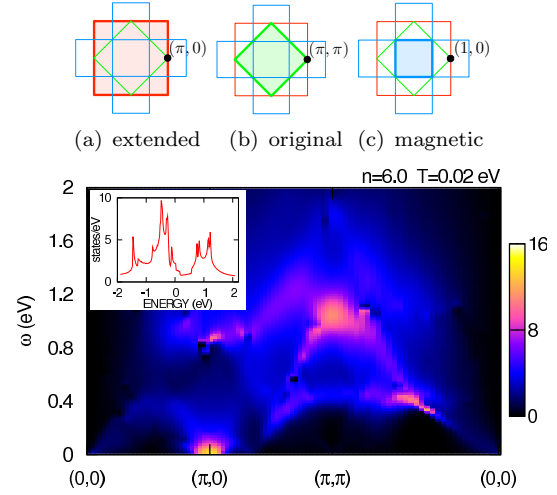


Fig. 1. (Color online) Overall view of $S(\mathbf{q}, \omega)$ along the high symmetry lines in the Brillouin zone at temperature $T = 0.02\text{eV}$. Inset shows DOS of the present model. The upper panels denote the Brillouin zone of the present model containing one Fe per unit cell (a), original Brillouin zone having two Fe per unit cell (b), and that in the magnetic phase (c).

tem. In principle, $S(\mathbf{q}, \omega)$ in an itinerant model has low-lying excitations for $0 \leq |\mathbf{q}| \leq 2k_F$. However, in the present model for iron-pnictides, there are disconnected small Fermi surfaces around $(0, 0)$ and around $(\pi, 0)$. In addition to this, since $2k_F$ is small, $S(\mathbf{q}, \omega)$ has a rather narrow column-like response at $(\pi, 0)$. Furthermore, the moderate strength of Coulomb interaction makes the response more sharper in RPA treatment. Actually, calculated peak width is estimated to be about 0.125 of the distance between $(0, 0)$ and $(\pi, 0)$ in the extended Brillouin zone (In Fig. 2, $S(\mathbf{q}, \omega')$ with $\omega' = 15\text{meV}$ is plotted as inset). This width is in fairly good agreement with experimentally observed width.²⁴⁾ Although the most reported data (not all²⁰⁾) are lower than about 25meV at present, we make a plot of the same data up to 300meV in the upper panel of Fig. 2. We can see that the peak intensity vanishes with increasing frequency in this energy range and also that the V-shape peak structure becomes visible above 0.1eV. Here, in comparing the calculated result with the experiments, we must note that the band renormalization effect is neglected within our RPA treatment. Thus, the actual energy range will be lower than that indicated in Fig. 2, since the dispersion relation is squished by the band renormalization effect. Since the obtained peak intensity is so prominent at $(\pi, 0)$, the result does not change if we take into account polycrystalline nature.

In order to obtain a clearer view, the ω -dependence of $S(\mathbf{Q}, \omega)$ at $\mathbf{Q} = (\pi, 0)$, is shown in the upper panel of Fig. 3. We can see that $S(\mathbf{Q}, \omega)$ grows gradually with decreasing temperature. To see this behavior, the temperature dependence of the peak intensity, i.e. $S(\mathbf{Q}, \omega')$

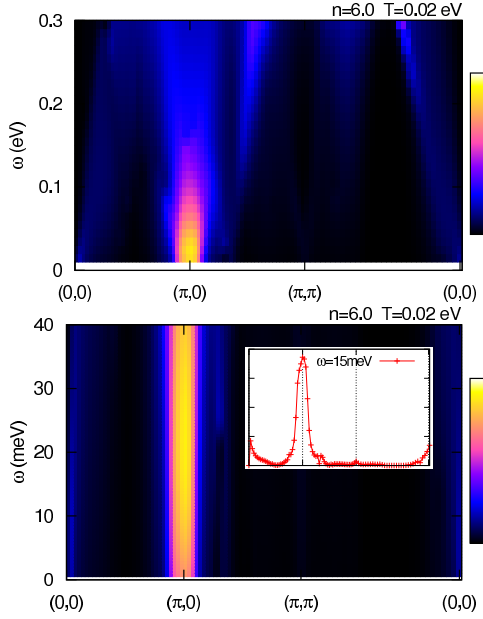


Fig. 2. (Color online) Low energy close-up of $S(\mathbf{q}, \omega)$ at temperature $T = 0.02\text{eV}$ (upper panel: up to 300meV , lower panel: up to 40meV). Inset: $S(\mathbf{q}, \omega')$ with $\omega' = 15\text{meV}$.

at $\omega' = 15\text{meV}$ is plotted in the inset of Fig. 3. This result is similar to the experimentally observed temperature dependence of the peak intensity above the ordering temperature.²³⁾ We also plot $\text{Im}\chi^{+-}(\omega, \mathbf{Q})/\omega$ in the lower panel of Fig. 3 to compare it with the other experiment by McQueeney *et al.*²¹⁾ This behavior is also consistent with the experimentally obtained result above ordering temperature,²¹⁾ considering the renormalization effect on energy scale. These results on temperature and frequency dependence is usual in RPA theory of magnetism. Here, we make a technical remark. Shown frequency dependence is obtained by Padé approximation, but we also calculate the same quantity in another method where analytic continuation is not needed. Two results are basically same, but Padé approximation gives a little smoother frequency dependence.

Here, we briefly explain how above picture would change with doping. With electron doping, the peak position around $\omega = 0$ shifts to the incommensurate position, where the peak of the static susceptibility is found.⁵⁾ Namely, the main peak shifts in the direction from $(\pi, 0)$ to (π, π) . As expected, the scattering intensity of the low energy excitations quickly weakens by doping since the doping breaks the nesting condition and brings the system away from the magnetic instability.

All the above results show that the itinerant model gives natural explanation for the neutron scattering experiments at least in the state without long-range order, although the sharp peak near $(\pi, 0)$ has been often analyzed by local spin models. Here, we want to make

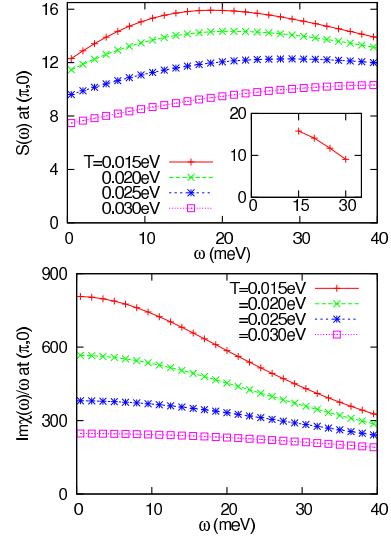


Fig. 3. (Color online) Frequency dependence of $S(\mathbf{Q}, \omega)$ (upper panel) and $\text{Im}\chi^{+-}(\mathbf{Q}, \omega)/\omega$ (lower panel) at $\mathbf{Q} = (\pi, 0)$ for several temperatures. Inset of upper panel: Temperature dependence of $S(\mathbf{Q}, \omega')$ at $\mathbf{Q} = (\pi, 0)$ and $\omega' = 15\text{meV}$. Note that horizontal axis of inset is temperature (meV).

some comments on the ordered state. First is about how $S(\mathbf{q}, \omega)$ looks like in the ordered state. If we consider only Stoner type excitations as in the previous treatment, and if there appears an SDW gap in the ordered state, low energy electronic excitation is removed and $S(\mathbf{q}, \omega)$ intensity drops for ω in the SDW gap. This scenario may explain the observed temperature dependence of peak intensity of $S(\mathbf{q}, \omega)$ shown in Ishikado *et al.*²³⁾ However, in the ordered state, we must consider collective excitations, i.e., spin wave, as well. Then, it is not so simple to reveal the actual shape of $S(\mathbf{q}, \omega)$ in the ordered phase. Second is about the order of the phase transition, i.e., second order or first order. In our treatment, or in the standard RPA approximation, transition becomes second order. However, in the actual compounds, lattice deformation is accompanied and this may bring the transition to first order. Third, the consideration on the three dimensionality is required to discuss the ordered phase precisely. However, as shown by Matan *et al.*,²⁴⁾ the spin dynamics is highly two dimensional above the ordering temperature, which justifies the present treatment.

Finally, we calculate the NMR result of $1/T_1T$ on the same footing, i.e., itinerant model and RPA approximation. Figure 4 shows the temperature dependence of $1/T_1T$ obtained in the present treatment. Actually, Ikeda has calculated the normal state $1/T_1T$ in the FLEX approximation, in which the self energy correction is also taken into account,³⁰⁾ and the arguments similar to our treatment are presented in Graser *et al.*³¹⁾ Thus, the present calculation for $1/T_1T$ is just for checking the parameter choice. The obtained result in Fig. 4 basically

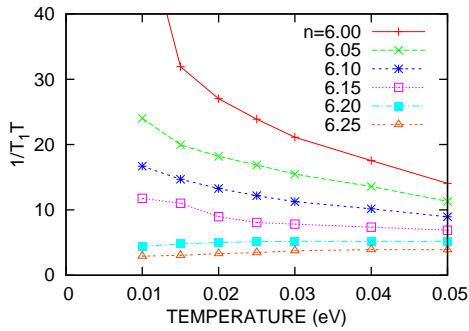


Fig. 4. (Color online) Temperature dependence of $1/T_1T$ for several doping levels.

captures the experimentally observed properties.^{12,19)} In the lower doping side, $1/T_1T$ shows enhancement with decreasing temperature due to the Fermi surface nesting. On the other hand, in the higher doping side, $1/T_1T$ shows slight decrease, which comes from the disappearance of the Fermi surface nesting as well as the DOS structure of this model. However, this result is not enough to explain the experiments quantitatively. One is about the doping dependence. In experiments, the behavior of $1/T_1T$ changes from increasing to decreasing more rapidly with doping. Another is about the behavior in the higher doping side. Observed decrease is more prominent than the present calculation, and shows one order drop from room temperature to superconducting transition temperature. Although the FLEX approximation³⁰⁾ gives a better result on this issue, the effects beyond the rigid band shift may be important.

In summary, it is shown that the itinerant model treated within RPA approximation can consistently explain the inelastic neutron scattering results such as peak width or temperature dependence of the peak intensity. The NMR results can be also roughly reproduced on the same footing, but quantitatively, it is not satisfactory yet. Although our conclusion is that the itinerant model reproduces normal state spin dynamics well (at least qualitatively), our calculation does not exclude the possibility of the localized-spin model. Further works will be necessary for determining whether the strong correlation and/or Mott insulating behavior is important in this iron-pnictide superconductors.

Acknowledgment

We thank T. J. Sato for stimulating discussions.

- 1) Y. Kamihara, T. Watanabe, M. Hirano, and H. Hosono: *J. Am. Chem. Soc.* **130** (2008) 3296.
- 2) Z. Ren, W. Lu, J. Yang, W. Yi, X. Shen, Z. Li, G. Che, X. Dong, L. Sun, F. Zhou, et al.: *Chin. Phys. Lett.* **25** (2008) 2215.
- 3) H. Kito, H. Eisaki, and A. Iyo: *J. Phys. Soc. Jpn* **77** (2008) 063707.

- 4) D. Singh and M. Du: *Phys. Rev. Lett.* **100** (2008) 237003.
- 5) K. Kuroki, S. Onari, R. Arita, H. Usui, Y. Tanaka, H. Kontani, and H. Aoki: *Phys. Rev. Lett.* **101** (2008) 087004.
- 6) S. Ishibashi, K. Terakura, and H. Hosono: *J. Phys. Soc. Jpn* **77** (2008) 053709.
- 7) D. Hsieh, Y. Xia, L. Wray, D. Qian, K. Gomes, A. Yazdani, G. Chen, J. Luo, N. Wang, and M. Hasan: arXiv:0812.2289.
- 8) A. Drew, F. Pratt, T. Lancaster, S. Blundell, P. Baker, R. Liu, G. Wu, X. Chen, I. Watanabe, V. Malik, A. Dubroka, K. Kim, M. Roessle, and C. Bernhard: *Phys. Rev. Lett.* **101** (2008) 097010.
- 9) Y. Yanagi, Y. Yamakawa, and Y. Ono: *J. Phys. Soc. Jpn* **77** (2008) 123701.
- 10) C. H. Lee, T. Ito, A. Iyo, H. Eisaki, H. Kito, M. T. Fernandez-Diaz, K. Kihou, H. Matsuhata, M. Braden, and K. Yamada: *J. Phys. Soc. Jpn* **77** (2008) 083704.
- 11) V. Vildosola, L. Pourovskii, R. Arita, S. Biermann, and A. Georges: *Phys. Rev. B* **78** (2008) 064518.
- 12) Y. Nakai, S. Kitagawa, K. Ishida, Y. Kamihara, M. Hirano, and H. Hosono: arXiv:0810.3569.
- 13) J. Checkelsky, L. Li, G. Chen, J. Luo, N. Wang, and N. Ong: arXiv:0811.4668.
- 14) K. Hashimoto, T. Shibauchi, T. Kato, K. Ikada, R. Okazaki, H. Shishido, M. Ishikado, H. Kito, A. Iyo, H. Eisaki, S. Shamoto, and Y. Matsuda: arXiv:0806.3149.
- 15) H. Ding, P. Richard, K. Nakayama, T. Sugawara, T. Arakane, Y. Sekiba, A. Takayama, S. Souma, T. Sato, T. Takahashi, Z. Wang, X. Dai, Z. Fang, G. F. Chen, J. L. Luo, and N. L. Wang: *Europhys. Lett.* **83** (2008) 47001.
- 16) A. S. Sefat, M. A. McGuire, R. Jin, B. C. Sales, and D. Mandrus: *Phys. Rev. Lett.* **101** (2008) 117004.
- 17) A. Kawabata, S. C. Lee, T. Moyooshi, Y. Kobayashi, and M. Sato: *J. Phys. Soc. Jpn* **77** (2008) 103704.
- 18) Y. Senga and H. Kontani: *J. Phys. Soc. Jpn* **77** (2008) 113710.
- 19) F. Ning, K. Ahilan, T. Imai, A. Sefat, R. Jin, M. McGuire, B. Sales, and D. Mandrus: arXiv:0811.1617.
- 20) R. A. Ewings, T. G. Perring, R. I. Bewley, T. Guidi, M. J. Pitcher, D. R. Parker, S. J. Clarke, and A. T. Boothroyd: *Phys. Rev. B* **78** (2008) 220501.
- 21) R. J. McQueeney, S. O. Diallo, V. P. Antropov, G. Samolyuk, C. Broholm, N. Ni, S. Nandi, M. Yethiraj, J. L. Zarestky, J. J. Pulikkotil, A. Kreyssig, M. D. Lumsden, B. N. Harmon, P. C. Canfield, and A. I. Goldman: arXiv:0809.1410.
- 22) J. Zhao, D.-X. Yao, S. Li, T. Hong, Y. Chen, S. Chang, W. Ratcliff II, J. W. Lynn, H. A. Mook, G. F. Chen, J. L. Luo, N. L. Wang, E. W. Carlson, J. Hu, and P. Dai: *Phys. Rev. Lett.* **101** (2008) 167203.
- 23) M. Ishikado, R. Kajimoto, S. Shamoto, M. Arai, A. Iyo, K. Miyazawa, P. M. Shirage, H. Kito, H. Eisaki, S. Kim, H. Hosono, T. Guidi, R. Bewley, and S. M. Bennington: arXiv:0809.5128.
- 24) K. Matan, R. Morinaga, K. Iida, and T. Sato: arXiv: 0810.4790.
- 25) G. Unrig, M. Holt, J. Oitmaa, O. Sushkov, and S. Rajiv: arXiv: 0810.3068.
- 26) D.-X. Yao and E. W. Carlson: *Phys. Rev. B* **78** (2008) 052507.
- 27) R. Liu, G. Wu, T. Wu, D. Fang, H. Chen, S. Li, K. Liu, Y. Xie, X. Wang, R. Yang, et al.: *Phys. Rev. Lett.* **101** (2008) 087001.
- 28) W. Malaeb, T. Yoshida, T. Kataoka, A. Fujimori, M. Kubota, K. Ono, H. Usui, K. Kuroki, R. Arita, H. Aoki, Y. Kamihara, M. Hirano, and H. Hosono: *J. Phys. Soc. Jpn* **77** (2008) 093714.
- 29) H. Ding, K. Nakayama, P. Richard, S. Souma, T. Sato, T. Takahashi, M. Neupane, Y. Xu, Z. Pan, A. Federov, et al.: arXiv:0812.0534.
- 30) H. Ikeda: *J. Phys. Soc. Jpn* **77** (2008) 123707.
- 31) S. Graser, T. Maier, P. Hirschfeld, and D. Scalapino: arXiv:0812.0343.